Phase-Sensitive Quantum Measurement without Controlled Operations

Yilun Yang,[1, 2] Arthur Christianen,[1, 2] Mari Carmen Bañuls,[1, 2] Dominik S. Wild,[1, 2] and J. Ignacio Cirac[1, 2]

[1] *Max-Planck-Institut für Quantenoptik, Hans-Kopfermann-Str. 1, D-85748 Garching, Germany*
[2] *Munich Center for Quantum Science and Technology (MCQST), Schellingstr. 4, D-80799 München*

(Dated: August 22, 2023)

Many quantum algorithms rely on the measurement of complex quantum amplitudes. Standard approaches to obtain the phase information, such as the Hadamard test, give rise to large overheads due to the need for global controlled-unitary operations. We introduce a quantum algorithm based on complex analysis that overcomes this problem for amplitudes that are a continuous function of time. Our method only requires the implementation of real-time evolution and a shallow circuit that approximates a short imaginary-time evolution. We show that the method outperforms the Hadamard test in terms of circuit depth and that it is suitable for current noisy quantum computers when combined with a simple error-mitigation strategy.

Introduction.— The complex phases of quantum amplitudes play an essential role in quantum algorithms [1–5] and quantum sensing [6]. Many algorithms require measuring the relative phase between two quantum states [7–14]. A common subroutine for this purpose is the Hadamard test, which converts phase information into probabilities by means of interference [15]. Despite impressive experimental progress, the Hadamard test remains out of reach for most applications owing to the challenge of implementing the required controlled-unitary operation. In this Letter, we propose an alternative method to determine the complex overlap between certain states that uses no ancillary qubits or global controlled-unitary operations. Unlike other ancilla-free schemes [11, 16], our approach does not require the preparation of superpositions with a reference state, which are highly susceptible to noise [17–22]. Instead of interference, our method hinges on the principles of complex analysis.

The proposed approach applies to overlaps of the form of the (generalized) Loschmidt amplitude

$$\mathcal{G}(t) = \langle\psi'|e^{-iHt}|\psi\rangle, \tag{1}$$

where H is a local Hamiltonian and $|\psi\rangle$ is a state with a short correlation length, such as a product state or a state prepared with a short-depth circuit. We assume that an efficient projective measurement onto $|\psi'\rangle$ is available [23]. The absolute value $|\mathcal{G}(t)|$ can be obtained by repeatedly evolving $|\psi\rangle$ and averaging over projective measurements onto $|\psi'\rangle$. Here we describe how to obtain the phase.

Equation (1) includes several cases of interest. When $|\psi'\rangle = |\psi\rangle$, $\mathcal{G}(t)$ is the Fourier transform of the local density of states, which has applications in the study of quantum chaos [24, 25], in optimal measurements of multiple expectation values [13], and in estimating energy eigenvalues [8, 9, 12]. The case when $|\psi'\rangle = Ae^{-iHt'}|\psi\rangle$, for a local unitary A, is relevant for probing thermal properties of many-body systems [11].

The key idea underlying our method is to view $\mathcal{G}$ as a function of a complex variable z. Assuming that $\mathcal{G}(z)$
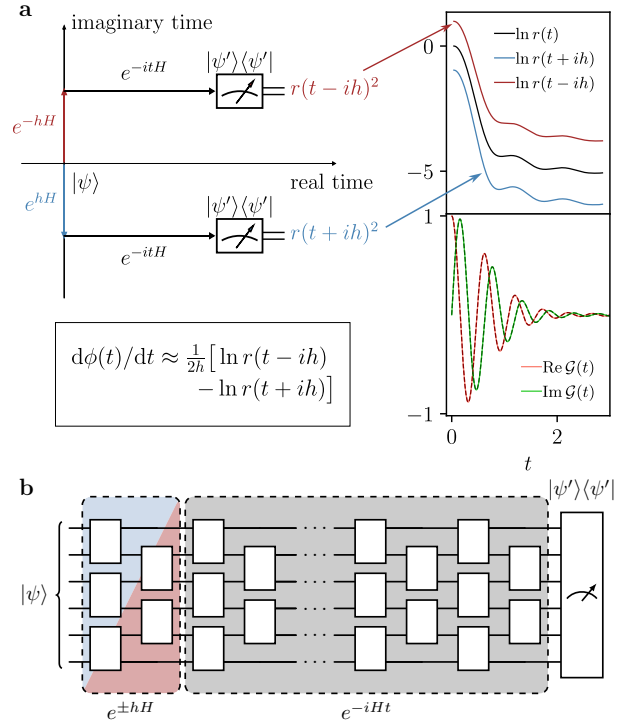

FIG. 1. **(a)** The time derivative of the complex phase $\phi(t)$ of the Loschmidt amplitude $\mathcal{G}(t)$ can be estimated from $r(t \pm ih) = |\langle\psi'|e^{-iHt}e^{\pm hH}|\psi\rangle|$. The right panel shows the result of our approach with $h = 0.1$ for the transverse-field Ising chain, Eq. (8), of length $N = 40$. The solid lines on the lower right correspond to the complex Loschmidt amplitude obtained from the algorithm, while the overlapping dashed lines indicate the exact result. **(b)** Circuit to measure $r(t \pm ih)$. For initial product states, the rescaled imaginary-time evolution has the same brickwork layout as a single real-time Trotter step.

is analytic and nonzero, the Cauchy-Riemann equations imply that the real-time derivative of the phase of $\mathcal{G}(z)$ is equal to the derivative of $\ln|\mathcal{G}(z)|$ along the imaginary-time direction. We use this relation to obtain the desired phase by carrying out the following three steps on a quan-

tum computer (see Fig. 1). First, a quantum circuit applies an evolution under the Hamiltonian H for a short *imaginary time h* to the initial state $|\psi\rangle$ [26–31]. Second, we evolve the system under H for the *real time t*. Third, we perform a projective measurement onto the state $|\psi'\rangle$. Using these steps, we can estimate $|\mathcal{G}(t \pm ih)|$. This yields a finite-difference approximation to the imaginary-time derivative of $\ln|\mathcal{G}(z)|$, which is equal to the real-time derivative of the phase. We finally compute the phase of the Loschmidt amplitude by repeating these steps for different values of t and numerically integrating the derivative, starting from a time at which the phase is known.

We show below that our method is efficient if $|\mathcal{G}(t \pm ih)|$ is bounded from below by an inverse polynomial in the system size N. For product states $|\psi'\rangle = |\psi\rangle$, however, the Loschmidt amplitude decays as a Gaussian function on a time scale $\mathcal{O}(1/\sqrt{N})$ [32]. In this case, our approach will be inefficient even for short constant times, for which the Loschmidt amplitude can be computed by a polynomial-time, classical algorithm [33]. By contrast, no efficient classical algorithm is known for the case $|\psi'\rangle = Ae^{-iHt'}|\psi\rangle$. Since the real- and imaginary-time evolution operators commute, our method can be used to compute the phase as a function of $t - t'$, with the expectation value $\langle\psi|e^{iHt'}Ae^{-iHt'}|\psi\rangle$ serving as the reference for the integration. This is expected to be classically hard even for small $t - t'$ since computing the reference value at times $t' = \text{poly}(N)$ is BQP-complete [34].

Although our approach is based on the analytic properties of a function of a continuous variable, we show below that it also works well in the discrete setting of Trotter evolution. Hence, the method applies to both circuit-based quantum computers and to analog quantum simulators supplemented by shallow circuits to implement the imaginary-time evolution. To demonstrate the suitability of the method for near-term quantum devices, we combine it with a simple error-mitigation strategy [35–40] and show numerically that the phase can be reliably recovered in a system of $N = 24$ qubits. Beyond providing a viable alternative to the Hadamard test on near-term quantum computers, our method may be useful in the early fault-tolerant regime as the absence of controlled global operations significantly reduces the circuit depth.

Theoretical approach.— To formally describe the algorithm, we consider the complex variable $z = t - i\beta$, where t represents real time and β stands for imaginary time or inverse temperature. The generalized Loschmidt amplitude, Eq. (1), can be decomposed into its absolute value and phase according to

$$\mathcal{G}(z) = r(z)e^{i\phi(z)}, \qquad (2)$$

where $0 \leq r(z) \leq 1$ and $\phi(z)$ is real. In a system of finite size, the Loschmidt amplitude can be written as a sum of exponentials by expanding the states $|\psi\rangle$ and $|\psi'\rangle$ in the energy eigenbasis. The logarithm $\ln\mathcal{G}(z)$ is therefore holomorphic everywhere except when $\mathcal{G}(z) = 0$. For an

analytic branch of $\phi(z)$, the Cauchy-Riemann equations applied to $\ln\mathcal{G}(z) = \ln r(z) + i\phi(z)$ give

$$\frac{\partial}{\partial t}\phi(z) = \frac{\partial}{\partial\beta}[\ln r(z)]. \qquad (3)$$

Therefore, if $\mathcal{G}(t) \neq 0$ in the interval $[t_1, t_2]$, the phase difference $\phi(t_2) - \phi(t_1)$ can be computed as

$$\phi(t_2) - \phi(t_1) = \int_{t_1}^{t_2} \frac{\partial}{\partial\beta}[\ln r(z)]_{|\beta=0}\, \mathrm{d}t. \qquad (4)$$

If the phase $\phi(t_1)$ is known, then $\phi(t_2)$ may be computed from the partial derivative of $r(z)$ along the imaginary-time direction. In practice, we numerically approximate the partial derivative by the mid-point formula

$$\frac{\partial}{\partial\beta}[\ln r(z)]_{|\beta=0} \approx \frac{\ln r(t - ih) - \ln r(t + ih)}{2h}, \qquad (5)$$

where h is a small parameter.

This procedure is well defined for $r(t \pm ih) > 0$ in the interval $[t_1, t_2]$. To bound the computational errors, we make the stronger assumption that $|\ln r(z)| \leq cN$ at all points in the complex plane within distance a of the interval $[t_1, t_2]$, for constants c and $a > h$. In the case of Trotter evolution, we make analogous assumptions for closely related functions [41]. We highlight, however, that our approach can be extended to treat zeros in $\mathcal{G}(t)$ by separately considering the resulting discontinuities in the phase [41].

The above analysis has reduced the problem to measuring the absolute values $r(t \pm ih)^2$. It involves nonunitary imaginary-time evolution which cannot be directly applied. However, Motta *et al.* [27] showed that $e^{\pm hH}$ can be simulated by a shallow-depth circuit for short times h if $|\psi\rangle$ has finite correlation length ξ and H is a local Hamiltonian [27]. Since h is small, we may use a first-order Trotter decomposition to approximate $e^{\pm hH} \approx \prod_m e^{\pm hH_m}$, where H_m is a local operator that acts on at most k sites. It is possible to approximate $e^{\pm hH_m}|\psi\rangle \approx c_m^\pm V_m^\pm|\psi\rangle$, where $V_m^\pm$ is a unitary operator acting on $\mathcal{O}(\xi^d)$ qubits in d spatial dimensions. The factor $c_m^\pm = \sqrt{\langle\psi|e^{\pm 2hH_m}|\psi\rangle}$ accounts for the normalization. Both $c_m^\pm$ and $V_m^\pm$ can be determined by local measurements of the state $|\psi\rangle$.

Below, we focus on product initial states, for which $V_m^\pm$ can be chosen to act on the same sites as the Hamiltonian terms H_m. The resulting circuit has the same brickwork layout as a single real-time Trotter step, although the local unitary operations may be more complex.

Error analysis.— We next analyze the error in the estimated phase arising from the different approximations in our algorithm. The approximation error of the imaginary-time evolution is dominated by the first-order Trotter decomposition, which results in the phase error [41]

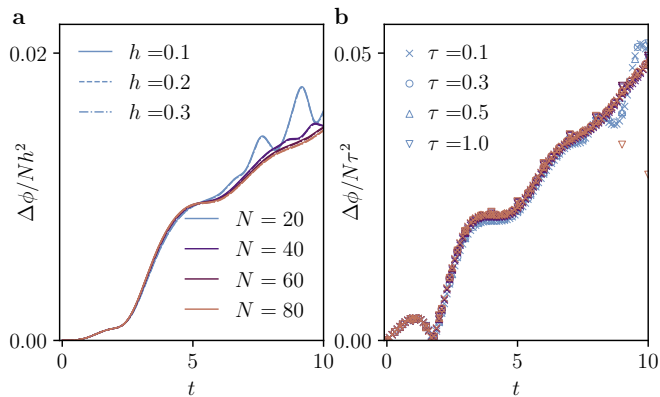$$\Delta\phi_{\text{ITE}} = \mathcal{O}(Nth^2). \qquad (6)$$

FIG. 2. Error in the phase of the Loschmidt amplitude, $\Delta\phi$, computed using our approach for the transverse-field Ising chain, Eq. (8). **(a)** $\Delta\phi/Nh^2$ as a function of time t with fixed real-time Trotter step $\tau = 0.01$ for different values of the imaginary-time step h and different system sizes N. **(b)** $\Delta\phi/N\tau^2$ for $h = 0.01$ and different values of τ and N. The color coding is the same as in (a).

The factor $t = t_2 - t_1$ accounts for the accumulation of errors in the integral in Eq. (4). While the real-time evolution can be carried out exactly on analog quantum simulators, digital quantum computers incur an additional Trotter error, leading to the phase error [41]

$$\Delta\phi_{\mathrm{RTE}} = \mathcal{O}(Nt^2\tau^p). \tag{7}$$

Here, τ is the time of a single Trotter step, p is the order of the Trotter decomposition [42], and we again included the accumulation of errors in Eq. (4). Numerical differentiation and integration give rise to additional errors. They can, however, be safely ignored for practical orders of the Trotter expansion ($p \leq 4$) as they are asymptotically at most as big as $\Delta\phi_{\mathrm{ITE}}$ and $\Delta\phi_{\mathrm{RTE}}$ [41].

We verify these analytic estimates using numerical results for the transverse-field Ising chain, whose Hamiltonian is given by

$$H = -J \sum_{i=1}^{N-1} S_i^z S_{i+1}^z + g \sum_{i=1}^{N} S_i^x. \tag{8}$$

Throughout this work, we set $J = 1$ and $g = 0.5$, corresponding to the ferromagnetic phase. The states $|\psi\rangle$ and $|\psi'\rangle$ are both chosen to be the product state $|\uparrow\uparrow\uparrow\cdots\rangle$. For the Trotter decomposition, we alternate between the ferromagnetic and transverse field terms.

Figure 2 shows the error in the phase computed using our approach. The numerical results were obtained by matrix product state simulations with bond dimension 200, for which truncation errors are negligible [41]. In Fig. 2(a), we set $\tau = 0.01$ such that the error in the imaginary-time evolution dominates. The phase error collapses onto a single curve upon dividing by Nh^2, which confirms the predicted error due to the imaginary-time

Method	D	M
Hadamard test	$\mathcal{O}(t^{1+\frac{1}{p}}N^{1+\frac{1}{d}+\frac{1}{p}}/\epsilon^{\frac{1}{p}})$	$\mathcal{O}(1/\epsilon^2)$
Sequential interferometry	$\mathcal{O}(r^{\frac{1}{p}}t^{1+\frac{1}{p}}N^{\frac{2}{p}}/\epsilon^{\frac{1}{p}})$	$\mathcal{O}(\tilde{I}^2 r^2 N^2/\epsilon^2)$
This work	$\mathcal{O}(r^{\frac{1}{p}}t^{1+\frac{2}{p}}N^{\frac{1}{p}}/\epsilon^{\frac{1}{p}})$	$\mathcal{O}\left(I^2 r^3 t^3 N/\epsilon^3\right)$

TABLE I. Circuit depth D and number of measurements M to estimate the complex Loschmidt amplitude $\mathcal{G}$ with additive error ϵ. All protocols use a real-time Trotter decomposition of order p. The Hadamard test is implemented using a single ancilla qubit with swap operations in d spatial dimensions. The latter two methods require M measurements at each intermediate state or time step, but the corresponding values of the phase are also returned. The quantities $\tilde{I}$ and I depend on the intermediate amplitudes in these sequences, see text and supplemental material [41]. For these approaches, we only consider the error $r\Delta\phi$ arising from the uncertainty in the phase.

evolution, Eq. (6). Similarly, we set $h = 0.01$ in Fig. 2(b) to isolate the effect of the real-time Trotter error. The collapse of the data agrees with Eq. (7).

In addition to numerical errors, any experiment incurs statistical errors. Given M measurements, a probability p estimated by counting successful outcomes will have a multiplicative error $\sqrt{(1-p)/Mp}$, governed by the standard deviation of the binomial distribution. According to Eq. (5), for the measured probabilities $p_{\pm}(t) = r(t \pm ih)^2/\prod_m(c_m^{\pm})^2$, this contributes an additive error

$$\Delta\phi_{\mathrm{S}} = \mathcal{O}\left(\frac{It}{h\sqrt{M}}\right) \tag{9}$$

to the final phase for M measurements per time step. The integral in Eq. (4) is included in the factor $I = \int_{t_1}^{t_2} dt' \left[\sqrt{1/p_+(t')} + \sqrt{1/p_-(t')}\right]/t$. In contrast to the previous errors, the statistical error depends on the magnitude of the measured probabilities.

Comparison with existing methods.— To compare our approach to existing methods, we consider the error $\Delta\mathcal{G}$ in the complex Loschmidt amplitude $\mathcal{G}$. This error is related to the phase error, $\Delta\phi$, by $|\Delta\mathcal{G}|^2 = \Delta r^2 + (r\Delta\phi)^2$. Here, Δr is the error from an independent measurement of r, which only requires the Trotterized circuit without imaginary-time evolution. To bound Δr by ϵ, we need a circuit of depth $D_r = \mathcal{O}(t/\tau) = \mathcal{O}(t^{1+\frac{1}{p}}N^{\frac{1}{p}}/\epsilon^{\frac{1}{p}})$ and a number of $M_r = \mathcal{O}\left(1/\epsilon^2\right)$ measurements [41]. For the term $r\Delta\phi$, we bound the individual contributions to the phase error. For instance, $r\Delta\phi_{\mathrm{ITE}} < \epsilon$ implies that $h = \mathcal{O}(\sqrt{\epsilon/rNt})$. A similar bound on the real-time evolution gives $\tau = \mathcal{O}((\epsilon/rNt^2)^{\frac{1}{p}})$, resulting in the circuit depth $D = \mathcal{O}(r^{\frac{1}{p}}t^{1+\frac{2}{p}}N^{\frac{1}{p}}/\epsilon^{\frac{1}{p}})$. Bounding the statistical error yields the number of measurements $M = \mathcal{O}(I^2 r^3 t^3 N/\epsilon^3)$ for each time step. We note that when r is bounded from below by a constant, the cost of estimating ϕ dominates.
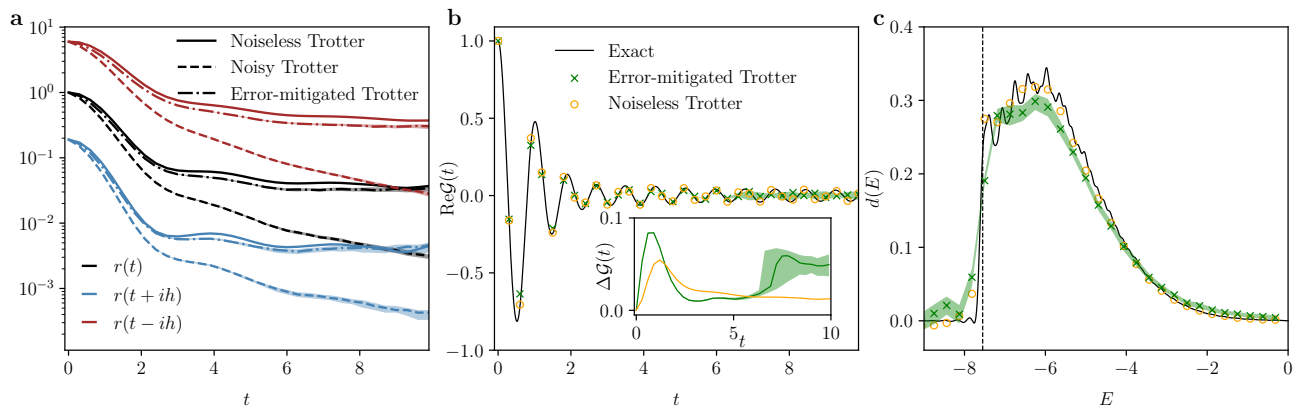
FIG. 3. **(a)** Absolute value of the Loschmidt amplitudes for an Ising chain of length $N = 24$ with initial state $|\uparrow\uparrow\uparrow\cdots\rangle$ and Trotter step sizes $\tau = h = 0.3$. The dashed lines include single-qubit depolarizing noise with probability $\gamma = 3 \times 10^{-3}$ after each gate. The dash-dotted lines are obtained by the error mitigation described in the text. We quantify the statistical error of the error-mitigated curves by simulating 100 experiments, each of which uses $M = 10^6$ measurements to estimate the survival probability. The dash-dotted line corresponds to the median of the 100 experiments, while the shaded areas indicate the range between the first and third quartile. **(b)** Real part of the Loschmidt amplitude computed from the data in (a) using our algorithm. The exact value under continuous time evolution is plotted for reference. The inset shows the absolute difference of the reconstructed values from the exact amplitude. **(c)** The LDOS obtained through discrete Fourier transform from the data in (b). The vertical, dashed line indicates the exact ground state energy $E_0 \approx -7.55$.

We compare this resource cost to the Hadamard test and to sequential interferometry [11]. The latter method employs a reference state whose Loschmidt amplitude, including the phase, is known. The details of these two methods are described in the supplemental material [41]. Table I summarizes the resource cost for each method. For a constant evolution time t, the circuit depth needed for our algorithm is reduced by a factor $\mathcal{O}(N^{1+1/d})$ compared to the Hadamard test with swaps, and by $\mathcal{O}(N^{1/p})$ compared to sequential interferometry. This improvement is of particular significance for noisy quantum computers, for which circuit depth is the key limiting factor.

Applications.— For practical applications of our protocol, it is important to consider the role of noise. We propose a simple rescaling strategy based on previous work to mitigate the effects of noise [40]. The key observation is that errors are unlikely to drive the system towards the target state $|\psi'\rangle$. Hence, the measured probabilities are decreased in a consistent fashion, which can be mitigated by rescaling with the probability of having no noise. This is equivalent to zero-noise extrapolation with an exponential fitting function [35, 43, 44]. Below, we simply use the known noise rate for rescaling. In practice, the rescaling factor can be determined by enhancing the noise or by measuring the survival probability after forward plus backward evolution [40].

As a proof of concept, we apply our approach to compute the local density of states (LDOS) $d(E)$ through the Fourier transform

$$d(E) = \langle\psi|\delta(E - H)|\psi\rangle = \frac{1}{2\pi} \int_{-\infty}^{\infty} \mathcal{G}(t)e^{iEt}\, dt. \quad (10)$$

The LDOS features prominently in Fermi's golden rule

and can be used to compute thermal properties of quantum many-body systems [11]. If the initial state has a sufficiently large overlap with the ground state, the LDOS enables the determination of the ground-state energy [10, 12].

We apply our approach to compute the LDOS of the state $|\uparrow\uparrow\uparrow\cdots\rangle$ in an Ising chain of system size $N = 24$. We numerically carry out the Trotter evolution with Trotter steps $\tau = h = 0.3$ using the Cirq library [45]. For noisy simulations, we add single-qubit depolarizing noise of rate $\gamma = 3 \times 10^{-3}$ after each layer of the quantum circuit. We average over 5000 trajectories of a Monte Carlo wavefunction simulation to obtain the probabilities $p_\pm$. To quantify the impact of statistical noise, we simulate an experiment by drawing $M = 10^6$ samples from a binomial distribution for each probability and taking the average. We generate 100 such experiments, whose median as well as the first and third quartiles are plotted as shaded areas in Fig. 3.

Figure 3(a) shows that the depolarizing noise is mitigated well by rescaling $r^2(t)$ and $r^2(t \pm ih)$ by $(1 - \gamma)^{ND}$. The error in the reconstructed Loschmidt amplitude remains small within the range of t in Fig. 3(b). We estimate the LDOS of the initial state by a discrete Fourier transform of the data in Fig. 3(b) and similar data for the imaginary part of $\mathcal{G}(t)$. The energy resolution is $\pi/t_{\max} \approx 0.31$, determined by the maximum time $t_{\max} = 10$. We show the result in Fig. 3(c) for both noisy, error-mitigated (green) and noiseless (orange) Trotter simulations. For reference, we also include the exact result (black line), which is broadened by a Gaussian of width 0.08. For both Trotter simulations, the first

point with $d(E) > 0.1$ appears at $E \approx -7.50$, while the exact ground state energy is $E_0 \approx -7.55$.

Summary and outlook.— We propose a quantum algorithm to estimate the phase of Loschmidt amplitudes. It can replace and outperform the Hadamard test for amplitudes that arise from continuous time evolution under a local Hamiltonian. While our analysis focused on generalized Loschmidt amplitudes, the approach can be readily extended to multiple time-evolution operators [41], which renders it applicable to many quantities of physical interest including out-of-time-ordered correlators (OTOCs) [46, 47]. The algorithm requires no ancillary qubits or controlled operations. When combined with a simple error-mitigation strategy, our algorithm may enable phase-sensitive measurements on current noisy quantum devices for system sizes that out of reach for other methods.

[1] P. Shor, Algorithms for quantum computation: discrete logarithms and factoring, in *Proceedings 35th Annual Symposium on Foundations of Computer Science* (1994) pp. 124–134.

[2] A. Y. Kitaev, Quantum measurements and the abelian stabilizer problem (1995), arXiv:quant-ph/9511026 [quant-ph].

[3] E. Knill, G. Ortiz, and R. D. Somma, Optimal quantum measurements of expectation values of observables, Physical Review A **75**, 012328 (2007).

[4] A. W. Harrow, A. Hassidim, and S. Lloyd, Quantum algorithm for linear systems of equations, Phys. Rev. Lett. **103**, 150502 (2009).

[5] N. Wiebe and C. Granade, Efficient bayesian phase estimation, Phys. Rev. Lett. **117**, 010503 (2016).

[6] C. L. Degen, F. Reinhard, and P. Cappellaro, Quantum sensing, Rev. Mod. Phys. **89**, 035002 (2017).

[7] D. Aharonov, V. Jones, and Z. Landau, A polynomial quantum algorithm for approximating the jones polynomial (Association for Computing Machinery, New York, NY, USA, 2006) p. 427–436.

[8] T. E. O'Brien, B. Tarasinski, and B. M. Terhal, Quantum phase estimation of multiple eigenvalues for small-scale (noisy) experiments, New Journal of Physics **21**, 023022 (2019).

[9] R. D. Somma, Quantum eigenvalue estimation via time series analysis, New Journal of Physics **21**, 123025 (2019).

[10] S. McArdle, S. Endo, A. Aspuru-Guzik, S. C. Benjamin, and X. Yuan, Quantum computational chemistry, Rev. Mod. Phys. **92**, 015003 (2020).

[11] S. Lu, M. C. Bañuls, and J. I. Cirac, Algorithms for quantum simulation at finite energies, PRX Quantum **2**, 020321 (2021).

[12] L. Lin and Y. Tong, Heisenberg-limited ground-state energy estimation for early fault-tolerant quantum computers, PRX Quantum **3**, 010318 (2022).

[13] W. J. Huggins, K. Wan, J. McClean, T. E. O'Brien, N. Wiebe, and R. Babbush, Nearly Optimal Quantum Algorithm for Estimating Multiple Expectation Values, Physical Review Letters **129**, 240501 (2022).

[14] T. L. Patti, J. Kossaifi, A. Anandkumar, and S. F. Yelin, Quantum Goemans-Williamson Algorithm with the Hadamard Test and Approximate Amplitude Constraints, Quantum **7**, 1057 (2023).

[15] R. Cleve, A. Ekert, C. Macchiavello, and M. Mosca, Quantum algorithms revisited, Proceedings of the Royal Society of London. Series A: Mathematical, Physical and Engineering Sciences **454**, 339 (1998).

[16] A. E. Russo, K. M. Rudinger, B. C. A. Morrison, and A. D. Baczewski, Evaluating energy differences on a quantum computer with robust phase estimation, Phys. Rev. Lett. **126**, 210501 (2021).

[17] R. Laflamme, E. Knill, W. H. Zurek, P. Catasti, and S. V. S. Mariappan, NMR Greenberger–Horne–Zeilinger states, Philosophical Transactions of the Royal Society of London. Series A: Mathematical, Physical and Engineering Sciences **356**, 1941 (1998).

[18] D. Leibfried, E. Knill, S. Seidelin, J. Britton, R. B. Blakestad, J. Chiaverini, D. B. Hume, W. M. Itano, J. D. Jost, C. Langer, R. Ozeri, R. Reichle, and D. J. Wineland, Creation of a six-atom 'Schrödinger cat' state, Nature **438**, 639 (2005).

[19] C. Song, K. Xu, W. Liu, C.-p. Yang, S.-B. Zheng, H. Deng, Q. Xie, K. Huang, Q. Guo, L. Zhang, P. Zhang, D. Xu, D. Zheng, X. Zhu, H. Wang, Y.-A. Chen, C.-Y. Lu, S. Han, and J.-W. Pan, 10-qubit entanglement and parallel logic operations with a superconducting circuit, Phys. Rev. Lett. **119**, 180511 (2017).

[20] A. Omran, H. Levine, A. Keesling, G. Semeghini, T. T. Wang, S. Ebadi, H. Bernien, A. S. Zibrov, H. Pichler, S. Choi, J. Cui, M. Rossignolo, P. Rembold, S. Montangero, T. Calarco, M. Endres, M. Greiner, V. Vuletić, and M. D. Lukin, Generation and manipulation of Schrödinger cat states in Rydberg atom arrays, Science **365**, 570 (2019).

[21] K. X. Wei, I. Lauer, S. Srinivasan, N. Sundaresan, D. T. McClure, D. Toyli, D. C. McKay, J. M. Gambetta, and S. Sheldon, Verifying multipartite entangled greenberger-horne-zeilinger states via multiple quantum coherences, Phys. Rev. A **101**, 032343 (2020).

[22] L. Bin, Y. Zhang, Q. P. Su, and C. P. Yang, Efficient scheme for preparing hybrid GHZ entangled states with multiple types of photonic qubits in circuit QED, Euro-

pean Physical Journal Plus **137**, 10.1140/epjp/s13360-022-03251-z (2022).

[23] The measurement is defined by a complete, mutually orthogonal set of projection operators that includes $|\psi'\rangle \langle\psi'|$. We assign $+1$ to an outcome of $|\psi'\rangle$ and 0 all other outcomes.

[24] G. Benenti and G. Casati, Quantum-classical correspondence in perturbed chaotic systems, Phys. Rev. E **65**, 066205 (2002).

[25] M. F. Andersen, A. Kaplan, T. Grünzweig, and N. Davidson, Decay of quantum correlations in atom optics billiards with chaotic and mixed dynamics, Phys. Rev. Lett. **97**, 104102 (2006).

[26] T. Jones, S. Endo, S. McArdle, X. Yuan, and S. C. Benjamin, Variational quantum algorithms for discovering hamiltonian spectra, Phys. Rev. A **99**, 062304 (2019).

[27] M. Motta, C. Sun, A. T. K. Tan, M. J. O'Rourke, E. Ye, A. J. Minnich, F. G. S. L. Brandão, and G. K.-L. Chan, Determining eigenstates and thermal states on a quantum computer using quantum imaginary time evolution, Nature Physics **16**, 205 (2020).

[28] S.-H. Lin, R. Dilip, A. G. Green, A. Smith, and F. Pollmann, Real- and imaginary-time evolution with compressed quantum circuits, PRX Quantum **2**, 010342 (2021).

[29] H. Nishi, T. Kosugi, and Y.-i. Matsushita, Implementation of quantum imaginary-time evolution method on NISQ devices by introducing nonlocal approximation, npj Quantum Inf. **7**, 85 (2021).

[30] P. Jouzdani, C. W. Johnson, E. R. Mucciolo, and I. Stetcu, Alternative approach to quantum imaginary time evolution, Phys. Rev. A **106**, 062435 (2022).

[31] H. Kamakari, S.-N. Sun, M. Motta, and A. J. Minnich, Digital quantum simulation of open quantum systems using quantum imaginary–time evolution, PRX Quantum **3**, 010320 (2022).

[32] M. Hartmann, G. Mahler, and O. Hess, Gaussian Quantum Fluctuations in Interacting Many Particle Systems, Letters in Mathematical Physics **68**, 103 (2004).

[33] D. S. Wild and A. M. Alhambra, Classical simulation of short-time quantum dynamics, PRX Quantum **4**, 020340 (2023).

[34] D. Janzing and P. Wocjan, Ergodic quantum computing, Quantum Inf. Process. **4**, 129 (2005).

[35] K. Temme, S. Bravyi, and J. M. Gambetta, Error mitigation for short-depth quantum circuits, Phys. Rev. Lett. **119**, 180509 (2017).

[36] S. Endo, S. C. Benjamin, and Y. Li, Practical quantum error mitigation for near-future applications, Phys. Rev. X **8**, 031027 (2018).

[37] A. Kandala, K. Temme, A. D. Córcoles, A. Mezzacapo, J. M. Chow, and J. M. Gambetta, Error mitigation extends the computational reach of a noisy quantum processor, Nature **567**, 491 (2019).

[38] T. E. O'Brien, S. Polla, N. C. Rubin, W. J. Huggins, S. McArdle, S. Boixo, J. R. McClean, and R. Babbush, Error mitigation via verified phase estimation, PRX Quantum **2**, 020317 (2021).

[39] Z. Cai, R. Babbush, S. C. Benjamin, S. Endo, W. J. Huggins, Y. Li, J. R. McClean, and T. E. O'Brien, Quantum error mitigation (2022), arXiv:2210.00921 [quant-ph].

[40] Y. Yang, A. Christianen, S. Coll-Vinent, V. Smelyanskiy, M. C. Bañuls, T. E. O'Brien, D. S. Wild, and J. I. Cirac, Simulating prethermalization using near-term quantum computers (2023), arXiv:2303.08461 [quant-ph].

[41] See supplementary material, which includes references [48–55], for I. analysis of errors; II. analysis of resource cost of different methods; III. approach to deal with discrete zeros in Loschmidt amplitude; IV. extension of the algorithm to multiple time evolution operators; and V. details in numerical simulations.

[42] A. M. Childs, Y. Su, M. C. Tran, N. Wiebe, and S. Zhu, Theory of trotter error with commutator scaling, Phys. Rev. X **11**, 011020 (2021).

[43] Y. Li and S. C. Benjamin, Efficient variational quantum simulator incorporating active error minimization, Phys. Rev. X **7**, 021050 (2017).

[44] Y. Kim, A. Eddins, S. Anand, K. X. Wei, E. van den Berg, S. Rosenblatt, H. Nayfeh, Y. Wu, M. Zaletel, K. Temme, and A. Kandala, Evidence for the utility of quantum computing before fault tolerance, Nature **618**, 500 (2023).

[45] Cirq Developers, Cirq (2022), See full list of authors on Github: https://github .com/quantumlib/Cirq/graphs/-contributors.

[46] K. Hashimoto, K. Murata, and R. Yoshii, Out-of-time-order correlators in quantum mechanics, Journal of High Energy Physics **2017**, 10.1007/JHEP10(2017)138 (2017).

[47] M. Sajjan, V. Singh, R. Selvarajan, and S. Kais, Imaginary components of out-of-time-order correlator and information scrambling for navigating the learning landscape of a quantum machine learning model, Phys. Rev. Res. **5**, 013146 (2023).

[48] A. Quarteroni, R. Sacco, and F. Saleri, *Numerical Mathematics* (Springer Berlin, Heidelberg, 2006).

[49] H. Touchette, The large deviation approach to statistical mechanics, Physics Reports **478**, 1 (2009).

[50] T. Monz, P. Schindler, J. T. Barreiro, M. Chwalla, D. Nigg, W. A. Coish, M. Harlander, W. Hänsel, M. Hennrich, and R. Blatt, 14-qubit entanglement: Creation and coherence, Phys. Rev. Lett. **106**, 130506 (2011).

[51] A. Gambassi and A. Silva, Large deviations and universality in quantum quenches, Phys. Rev. Lett. **109**, 250602 (2012).

[52] M. Heyl, A. Polkovnikov, and S. Kehrein, Dynamical quantum phase transitions in the transverse-field ising model, Phys. Rev. Lett. **110**, 135704 (2013).

[53] N. Friis, O. Marty, C. Maier, C. Hempel, M. Holzäpfel, P. Jurcevic, M. B. Plenio, M. Huber, C. Roos, R. Blatt, and B. Lanyon, Observation of entangled states of a fully controlled 20-qubit system, Phys. Rev. X **8**, 021012 (2018).

[54] A. Ozaeta and P. L. McMahon, Decoherence of up to 8-qubit entangled states in a 16-qubit superconducting quantum processor, Quantum Science and Technology **4**, 025015 (2019).

[55] A. W. Harrow, S. Mehraban, and M. Soleimanifar, Classical algorithms, correlation decay, and complex zeros of partition functions of quantum many-body systems, in *Proceedings of the 52nd Annual ACM SIGACT Symposium on Theory of Computing*, STOC 2020 (Association for Computing Machinery, New York, NY, USA, 2020) p. 378–386.

Supplemental Material

A. Errors

1. Zero-free functions

To apply our algorithm to the time interval $[t_1, t_2]$, we require that $\mathcal{G}(t)$ is nonzero in this region. In practice, we have to place a lower bound on the magnitude of $\mathcal{G}(t)$ to guarantee a bounded error of the algorithm. We will refer to functions that satisfy such a lower bound as zero free, following the terminology introduced in reference [55]. Owing to its similarity to the partition function, the Loschmidt amplitude generically takes the form $\mathcal{G}(z) \sim e^{-Ng(z)}$ in the limit of large N for some function $g(z)$ [49, 51, 52, 55]. This behavior motivates the following definition of a zero-free function.

Definition 1 (Zero-free functions). *A sequence of functions $f_N(z)$ on the complex plane is called zero free at point z_0 if there exist constants c and a such that $\log |f_N(z)| \leq cN$ for all z satisfying $|z - z_0| < a$.*

Assuming that a function is zero free allows us to bound to the derivatives of $\ln f_N(z)$ according to the following lemma.

Lemma 1. *Consider a sequence of holomorphic functions $f_N(z)$, which are zero free at $t_0 \in \mathbb{R}$. We let $z = t - i\beta$ with $t, \beta \in \mathbb{R}$ and $\log f_N(z) = \log r_N(z) + i\phi_N(z)$ for some analytic branch of the logarithm. Given any constant m, the magnitude of the partial derivatives $\partial^m \ln r_N(z)/\partial\beta^m$ and $\partial^m \phi_N(z)/\partial t^m$ at $z = t_0$ is bounded from above by $\mathcal{O}(N)$.*

Proof. To prove the lemma for $\partial^m \ln r_N(z)/\partial\beta^m$, we observe that

$$\frac{\mathrm{d}^m}{\mathrm{d}z^m} \ln f_N(z) = \frac{\partial^m}{\partial(-i\beta)^m} \ln r_N(z) + i\frac{\partial^m}{\partial(-i\beta)^m} \phi_N(z), \tag{A1}$$

which implies

$$\left| \frac{\partial^m}{\partial\beta^m} \ln r_N(t_0 - i\beta) \right|_{\beta=0} \leq \left| \frac{\mathrm{d}^m}{\mathrm{d}z^m} \ln f_N(z) \right|_{z=t_0}. \tag{A2}$$

The right-hand side can be expressed using Cauchy's integral formula as

$$\left| \frac{\mathrm{d}^m}{\mathrm{d}z^m} \ln f_N(z) \right|_{z=t_0} = \frac{m!}{2\pi} \left| \oint_{|\zeta|=a/2} \frac{\ln f_N(\zeta + t_0)}{\zeta^{m+1}} \mathrm{d}\zeta \right|. \tag{A3}$$

It remains to bound the magnitude of $\ln f_N(\zeta)$ on the circle $|\zeta - t_0| = a/2$. However, the magnitude depends on the choice of the branch of the logarithm. To overcome this issue, we consider the function $\tilde{f}_N(z) = e^{-i\phi_N(t_0)} f_N(z)$. We can bound the Cauchy integral (A3)

in terms of $\ln \tilde{f}_N(z)$ instead of $\ln f_N(z)$ because the derivatives of the two functions are equal.

To complete the bound, we use the Schwarz integral formula to express

$$\ln \tilde{f}_N(z + t_0) = \frac{1}{2\pi i} \oint_{|\zeta|=a} \frac{\mathrm{d}\zeta}{\zeta} \frac{\zeta + z}{\zeta - z} \operatorname{Re} \ln \tilde{f}_N(\zeta + t_0) + i \operatorname{Im} \ln \tilde{f}_N(t_0) \tag{A4}$$

for any $|z| < a$. Since $\operatorname{Im} \ln \tilde{f}_N(t_0) = 0$, this yields

$$|\ln \tilde{f}_N(z + t_0)| \leq \frac{a + |z|}{a - |z|} \max_{|\zeta|=a} |\operatorname{Re} \ln f_N(\zeta + t_0)| \tag{A5}$$

By assumption, we have

$$\max_{|\zeta|=a} |\operatorname{Re} \ln f_N(\zeta + t_0)| \leq cN. \tag{A6}$$

By substituting these results into (A2) and (A3), we obtain

$$\left| \frac{\partial^m}{\partial\beta^m} \ln r_N(t_0 - i\beta) \right|_{\beta=0} \leq \frac{m!cN}{2\pi} \oint_{|\zeta|=a/2} \frac{|\mathrm{d}\zeta|}{|\zeta|^{m+1}} \frac{a + |\zeta|}{a - |\zeta|}$$
$$\leq 3 \times 2^m m! \frac{c}{a^m} N \tag{A7}$$

For any constant value of m, the derivative of $\ln r_N$ is thus bounded by a quantity $\mathcal{O}(N)$.

The proof for $\partial^m \phi_N(z)/\partial t^m$ follows the same steps, starting from $|\partial^m \phi_N(t)/\partial t^m|_{t=t_0} \leq |\mathrm{d}^m/\mathrm{d}z^m \ln f_N(z)|_{z=t_0}$ in place of Eq. (A2). $\square$

For simplicity, we omit the subscript N below.

2. Error in numerical derivatives and integration

As a first illustration of the implications of the zero-free condition, let us deal with errors arising from numerical derivatives and integration. For the symmetric finite difference approximation to the derivative

$$\frac{\partial}{\partial\beta} \ln r(z)_{|\beta=0} \approx \frac{\ln r(t - ih) - \ln r(t + ih)}{2h}, \tag{A8}$$

the error is given by [48]

$$\Delta\phi_{\mathrm{D}} = \mathcal{O}(h^2) \cdot \left| \frac{\partial^3}{\partial\beta^3} [\ln r(z)]_{|\beta=0} \right| = \mathcal{O}(Nh^2), \tag{A9}$$

where the N dependence directly comes from Lemma 1, assuming that $\mathcal{G}(z)$ is zero free. This error will be multiplied by t in our algorithm, following the integration in Eq. (4) of the main text. We note that the error has the same scaling as the error $\Delta\phi_{\mathrm{ITE}}$ due to the approximate imaginary-time evolution. Therefore, a higher-order finite difference approximation will not improve the asymptotic scaling of the total error.

To compute the phase up to time t, we need to carry out the integral in Eq. (4) of the main text. In practice, we can only estimate the rate of change of the phase at a discrete set of points such that the integration is necessarily approximate. We use the Newton-Cotes formula of degree n with a fixed spacing τ between the samples, as is natural for a real-time Trotter step τ. The corresponding numerical integration error is [48]

$$\Delta\phi_{\mathrm{I}} = \mathcal{O}(t\tau^s) \max_{0 \le t' \le t} \left| \frac{\partial^s}{\partial t^s} \phi(t') \right| = \mathcal{O}(Nt\tau^s), \quad (A10)$$

where s equals $n + 2$ rounded down to the closest even number ($n = 1$, $s = 2$ for the trapezoidal rule; $n = 2$, $s = 4$ for Simpson's rule). The dependence on N again follows from Lemma 1. The Trotter error in the real-time evolution, $\Delta\phi_{\mathrm{RTE}}$, typically dominates over the error in the numerical integration, as the coefficient $s = 4$ for Simpson's rule exceeds the order p of practical low-order Trotter expansions.

3. Trotter errors

Trotter errors lead to an error in the estimation of the quantities

$$r(t \pm ih)^2 = \left| \langle \psi' | e^{-iHt} e^{\pm hH} | \psi \rangle \right|^2. \quad (A11)$$

The measured probabilities will have an *additive* Trotter error that scales as $\mathcal{O}(Nh^2)$ for imaginary-time evolution and as $\mathcal{O}(Nt\tau^p)$ for real-time evolution [42]. However, to bound the error on $\partial \ln r / \partial\beta$, it is necessary to control the *multiplicative* error in r. This is challenging because r may be exponentially small in the system size. Nevertheless, we show in this section that the above error scalings also apply to the numerical derivative in Eq. (A8) assuming that particular functions are zero free. We require that $\mathcal{G}(z)$, its Trotterized version $\mathcal{G}_{\mathrm{ITE}}(z)$ defined in Eq. (A14), and the function $\mathcal{F}_{t_0}(z, w)$ in Eq. (A23) are both zero free. We highlight that if these assumptions are violated, it may nevertheless be possible to compute the phase using the correction method described in Appendix C.

When expanded as the Taylor series in h, the finite difference in Eq. (A8) has the form

$$A(t, h) = \frac{\ln r(t - ih) - \ln r(t + ih)}{2h}$$
$$= \frac{\partial}{\partial\beta} \ln r(z)_{|\beta=0} + \frac{h^2}{6} \frac{\partial^3}{\partial\beta^3} \ln r(z)_{|\beta=0} + \mathcal{O}(h^3)$$
$$= \frac{\partial}{\partial\beta} \ln r(z)_{|\beta=0} + \mathcal{O}(Nh^2). \quad (A12)$$

The $\mathcal{O}(N)$ dependence in the last line comes again from applying Lemma 1 to $\mathcal{G}(z)$. We will us this form below.

For simplicity, we consider Trotter errors in the imaginary-time and real-time evolution separately. It is straightforward to show that the individual errors add when imaginary-time and real-time evolution are Trotterized at the same time.

a. Imaginary-time evolution

We consider a decomposition of the local Hamiltonian H into Γ terms,

$$H = \sum_{j=1}^{\Gamma} H_j. \quad (A13)$$

By replacing the exact imaginary-time evolution by the first-order Trotter decomposition $\prod_{j=1}^{\Gamma} e^{-hH_j}$, we obtain

$$\mathcal{G}_{\mathrm{ITE}}(t \pm ih) = \langle \psi' | e^{-iHt} \prod_{j=1}^{\Gamma} e^{\pm hH_j} | \psi \rangle \quad (A14)$$

and the corresponding finite difference approximation $A_{\mathrm{ITE}}(t, h)$.

According to the construction of Trotter decomposition, we have

$$\frac{\partial}{\partial\beta} \left(e^{\beta H} \right)_{|\beta=0} = \frac{\partial}{\partial\beta} \left(\prod_{j=1}^{\Gamma} e^{\beta H_j} \right)_{|\beta=0}, \quad (A15)$$

and thus

$$\frac{\partial}{\partial\beta} \ln r(z)_{|\beta=0} = \frac{\partial}{\partial\beta} \ln r_{\mathrm{ITE}}(z)_{|\beta=0}. \quad (A16)$$

If we also assume that $\mathcal{G}_{\mathrm{ITE}}$ is zero free at $z = t$, then using Lemma 1, the next nonzero term in the Taylor series reads

$$\frac{h^2}{6} \frac{\partial^3}{\partial\beta^3} \ln r_{\mathrm{ITE}}(z)_{|\beta=0} = \mathcal{O}(Nh^2). \quad (A17)$$

Hence,

$$A_{\mathrm{ITE}}(t, h) - A(t, h) = \mathcal{O}(Nh^2). \quad (A18)$$

b. Real-time evolution

For the real-time evolution, we consider

$$\mathcal{G}_{\mathrm{RTE}}(t \pm ih) = \langle \psi' | U_{\mathrm{RTE}}(t) e^{\pm hH} | \psi \rangle, \quad (A19)$$

where $U_{\mathrm{RTE}}(t) = U_p(t/D)^D$ is p-th order Trotter decomposition of the real-time evolution with a total number of D Trotter steps. We define the multiplicative error operator $M(t)$ by

$$U_{\mathrm{RTE}}(t) = [1 + M(t)]e^{-iHt}. \quad (A20)$$

The error operator is bounded in operator norm by $\|M(t)\| = \mathcal{O}(Nt\tau^p)$ [42], where $\tau = t/D$ [42].

We define $A_{\mathrm{RTE}}(t,h)$ as the approximation to the finite difference $A(t,h)$ with $r_{\mathrm{RTE}}(z) = |\mathcal{G}_{\mathrm{RTE}}(z)|$ in place of $r(z)$. The difference $A_{\mathrm{RTE}}(t,h) - A(t,h)$ is given by

$$\frac{1}{2}\frac{\partial}{\partial\beta}\ln g(z)_{|\beta=0} + \frac{h^2}{12}\frac{\partial^3}{\partial\beta^3}\ln g(z)_{|\beta=0} + \mathcal{O}(h^3), \text{ (A21)}$$

where

$$g(z) = \frac{r_{\mathrm{RTE}}(z)^2}{r(z)^2} = \left|1 + \frac{\langle\psi'|M(t)|\psi(z)\rangle}{\langle\psi'|\psi(z)\rangle}\right|^2, \quad \text{(A22)}$$

with $|\psi(z)\rangle = e^{-iHz}|\psi\rangle$. In contrast to the imaginary-time evolution, the first-order derivative does not cancel. It contributes the leading-order error, which we analyze in what follows.

We would like to again apply Lemma 1, which leads us to define

$$\mathcal{F}_{t_0}(z,w) = \langle\psi'|e^{M(t_0)w}|\psi(z)\rangle, \quad \text{(A23)}$$

where w is an independent complex variable from z. With this definition, $g(z) = |1 + \frac{\mathrm{d}}{\mathrm{d}w}(\ln\mathcal{F}_t)(z,0)|^2$. Let us assume that $\mathcal{F}_{t_0}(z,w)$ is zero-free for both z and w at $z = t_0$ and $w = 0$, i.e., $\ln|\mathcal{F}_{t_0}(z,w)| \le cN$ for all z,w such that $|z - t_0| < a_z$ and $|w| < a_w$. Since $\|M(t_0)\| = \mathcal{O}(Nt_0\tau^p)$, it is natural to choose $a_w = \mathcal{O}(1/(t_0\tau^p))$, while keeping $a_z = \mathcal{O}(1)$ and $c = \mathcal{O}(1)$. According to Lemma 1, we get $|\frac{\mathrm{d}}{\mathrm{d}w}(\ln\mathcal{F}_{t_0})(z,0)| = \mathcal{O}(N/a_w) = \mathcal{O}(Nt_0\tau^p)$. Assuming that $Nt_0\tau^p$ is small, it follows that $g(z) - 1 = \mathcal{O}(Nt_0\tau^p)$ to leading order for $|z - t_0| < a_z$.

Finally, we have to confirm that the partial derivative in Eq. (A21) does not change the system-size dependence. The leading term at $t = t_0$ is

$$\frac{1}{2}\frac{\partial}{\partial\beta}g(z)_{|z=t_0} \approx \mathrm{Re}\,\frac{\partial}{\partial\beta}\frac{\mathrm{d}}{\mathrm{d}w}\ln\mathcal{F}_{t_0}(z,w)_{|z=t_0,w=0}. \text{ (A24)}$$

Similar to the proof of Lemma 1, Eq. (A24) can be bounded as

$$\begin{aligned}
&\left|\mathrm{Re}\,\frac{\partial}{\partial\beta}\frac{\mathrm{d}}{\mathrm{d}w}\ln\mathcal{F}_{t_0}(z,w)_{|z=t_0,w=0}\right| \\
&\le \left|\frac{\mathrm{d}}{\mathrm{d}z}\frac{\mathrm{d}}{\mathrm{d}w}\ln\mathcal{F}_{t_0}(z,w)_{|z=t_0,w=0}\right| \\
&= \frac{1}{(2\pi)^2}\left|\oint_{|\zeta|=a_z/2}\oint_{|\eta|=a_w/2}\frac{\ln\mathcal{F}_{t_0}(\zeta+t_0,\eta)}{\zeta^2\eta^2}\mathrm{d}\zeta\mathrm{d}\eta\right| \\
&\le \frac{cN}{(2\pi)^2}\oint_{|\zeta|=a_z/2}\oint_{|\eta|=a_w/2}\frac{|\mathrm{d}\zeta||\mathrm{d}\eta|}{|\zeta\eta|^2}\cdot\frac{a_z+|\zeta|}{a_z-|\zeta|} \le \frac{12cN}{a_za_w}.
\end{aligned}$$
(A25)

Thus Eq. (A24) still scales as $cN/a_za_w = \mathcal{O}(Nt_0\tau^p)$ and we find that, to leading order,

$$A_{\mathrm{RTE}}(t,h) - A(t,h) = \mathcal{O}(Nt\tau^p). \quad \text{(A26)}$$

B. Resource cost

1. Estimating the magnitude r

An individual circuit to measure the magnitude r is required for our method and for sequential interferometry. It consists of Trotterized real-time evolution, which incurs a standard p-th order Trotter error [42] and statistical error

$$\Delta r = \mathcal{O}\left(Nt\tau^p + \frac{1}{\sqrt{M}}\right), \quad \text{(B1)}$$

where M is the number of measurements. To bound this error within ϵ, we require a circuit depth $D_r = \mathcal{O}(t/\tau) = \mathcal{O}(t^{1+\frac{1}{p}}N^{\frac{1}{p}}/\epsilon^{\frac{1}{p}})$ and the number of measurements $M_r = \mathcal{O}\left(1/\epsilon^2\right)$.
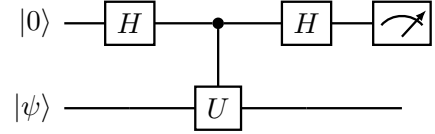
2. Hadamard test

FIG. 4. Quantum circuit diagram of the Hadamard test.

The Hadamard test is the standard method to compute the real and imaginary part of $\langle\psi|U|\psi\rangle$ for a given unitary U and initial state $|\psi\rangle$. The circuit of the Hadamard test is shown in Fig. 4. One first applies a Hadamard gate to an ancillary qubit. It is followed by a controlled unitary c-U acting on the prepared state $|\psi\rangle$ conditioned on the first ancillary qubit. Finally, apply the Hadamard gate again to the ancilla and measure this qubit. The probability of measuring 0 is

$$\frac{1 + \mathrm{Re}\,\mathcal{G}(t)}{2} = \frac{1 + r(t)\cos\phi(t)}{2}. \quad \text{(B2)}$$

To measure the imaginary part, we modify the circuit by adding a $S^\dagger = \begin{pmatrix} 1 & 0 \\ 0 & -i \end{pmatrix}$ gate after the first Hadamard gate.

It is hence possible to infer $\mathcal{G}(t)$ directly from the measured probabilities. Shot noise gives rise to the statistical error

$$\Delta\mathcal{G}_{\mathrm{S}}(t) = \mathcal{O}\left(1/\sqrt{M}\right), \quad \text{(B3)}$$

where M is the number of measurements. Compared to our proposed method, there is no need of integration, so the Trotter error does not have an additional t dependence:

$$\Delta\mathcal{G}_{\mathrm{RTE}}(t) = \mathcal{O}(Nt\tau^p). \quad \text{(B4)}$$

The total error is hence given by

$$\Delta\mathcal{G}(N,t,p,\tau,M) = \mathcal{O}\left(Nt\tau^p + \frac{1}{\sqrt{M}}\right). \qquad (B5)$$

Note that this only gives the phase of a single time t whereas our algorithm measures the phase on an interval $[0,t]$.

To bound the error $\Delta\mathcal{G} < \epsilon$, we need a Trotter step $\tau = \mathcal{O}((\epsilon/Nt)^{\frac{1}{p}})$ and a number of measurements $M = \mathcal{O}(1/\epsilon^2)$. If given access to global controlled unitary evolution, the corresponding circuit depth is $D = \mathcal{O}(t/\tau) = \mathcal{O}(t^{1+\frac{1}{p}}N^{\frac{1}{p}}/\epsilon^{\frac{1}{p}})$. However, on current devices usually only local gates are available. In this case there are two choices to implement this controlled unitary:

1. After Trotterization, swap the qubits of each local unitary next to the control qubit to perform local controlled evolution. The swapping process will increase the depth of circuit by $\mathcal{O}(N^{1+1/d})$ times, and thus $D = \mathcal{O}(t/\tau) = \mathcal{O}(t^{1+\frac{1}{p}}N^{1+\frac{1}{p}+\frac{1}{d}}/\epsilon^{\frac{1}{p}})$.

2. Distribute the control qubit onto a Greenberger–Horne–Zeilinger (GHZ) state of $\mathcal{O}(N)$ ancillary qubits [19–21, 50, 53]. This is, however, challenging on current devices due to the large decoherence rate of GHZ-states [50, 54].

3. Sequential interferometry

Suppose we know $\langle\psi_i|e^{-iHt}|\psi_i\rangle$ for some state $|\psi_i\rangle$. It is then possible to compute the Loschmidt amplitude $\langle\psi_j|e^{-iHt}|\psi_j\rangle$ by preparing superpositions of $|\psi_i\rangle$ and $|\psi_j\rangle$ with a tunable phase difference θ [11]. We denote $V_{ij}(\theta)$ a unitary that prepares such a state, i.e.,

$$V_{ij}(\theta)|\psi_i\rangle = \frac{1}{\sqrt{2}}\left(|\psi_i\rangle + e^{i\theta}|\psi_j\rangle\right). \qquad (B6)$$

For simplicity, we assume $|\psi_j\rangle$ is orthogonal to $|\psi_i\rangle$, although the procedure can be readily generalized to non-orthogonal states.

Let us introduce the notation

$$\langle\psi_x|e^{-iHt}|\psi_y\rangle = r_{xy}e^{i\phi_{xy}}. \qquad (B7)$$

We have access to all the r's from direct measurement of probabilities and we know ϕ_{ii} by assumption. The goal is to determine ϕ_{jj}. To do so, we can follow a two-step procedure:

1. Determine the phase of the cross term, $\phi_{ij} = -\phi_{ji}$. We need to measure

$$\left|\langle\psi_i|e^{-iHt}V_{ij}(\theta)|\psi_i\rangle\right|^2$$
$$= \frac{1}{2}\left[r_{ii}^2 + r_{ij}^2 + 2r_{ii}r_{ij}\cos(\phi_{ij}-\phi_{ii}+\theta)\right]. \qquad (B8)$$

In the case when $r_{ij} \neq 0$, only two different values of θ are needed to determine $\phi_{ij}-\phi_{ii}$ and thus ϕ_{ij}.

2. Now measure

$$\left|\langle\psi_j|e^{-iHt}V_{ij}(\theta)|\psi_i\rangle\right|^2$$
$$= \frac{1}{2}\left[r_{jj}^2 + r_{ij}^2 + 2r_{jj}r_{ij}\cos(\phi_{jj}-\phi_{ij}+\theta)\right]. \qquad (B9)$$

Again, two different value of θ are sufficient to determine ϕ_{jj}.

To prepare a global superposition state as in Eq. (B6) can be difficult. If the target state and the state for which the phase is known are both product states, it is possible to repeat the interferometry by flipping one or a few spins each time. Such a sequential approach requires only local gates. For a single call of this algorithm, the error in the phase difference $\phi_{jj} - \phi_{ii}$ is bounded by the error of extracting the phases in the terms $r_{ii}r_{ij}\cos(\phi_{ij}-\phi_{ii}+\theta)$ and $r_{jj}r_{ij}\cos(\phi_{jj}-\phi_{ij}+\theta)$. Hence, for a single step,

$$\Delta\phi = \mathcal{O}\left(Nt\tau^p + \frac{1}{\tilde{r}_{ij}^2\sqrt{M}}\right), \qquad (B10)$$

where

$$\frac{1}{\tilde{r}_{ij}^2} = \frac{1}{r_{ii}r_{ij}} + \frac{1}{r_{ij}r_{jj}}. \qquad (B11)$$

For the sequential version, on average $\mathcal{O}(N)$ calls are required for an arbitrary product state. Thus, the total phase error $\Delta\phi_N$ will be amplified as

$$\Delta\phi_N = \mathcal{O}\left(N^2t\tau^p + \frac{N\tilde{I}}{\sqrt{M}}\right), \qquad (B12)$$

where

$$\tilde{I} = \frac{1}{\lambda N}\sum_{i=0}^{\lambda N-1}\frac{1}{\tilde{r}_{i,i+1}^2}, \qquad (B13)$$

for a total number of λN steps in the sequence. We assume that $\lambda = \mathcal{O}(1)$ and omit it in Eq. (B12). Therefore, to control $r\Delta\phi_N$ within ϵ, one arrives at $D = \mathcal{O}(r^{\frac{1}{p}}t^{1+\frac{1}{p}}N^{\frac{2}{p}}/\epsilon^{\frac{1}{p}})$ and $M = \mathcal{O}(\tilde{I}^2r^2N^2/\epsilon^2)$.

We note that the above procedure fails when $r_{ij} \approx 0$. In this case, the following quantity is simplified as

$$\left|\langle\psi_i|V_{ij}^\dagger(0)e^{-iHt}V_{ij}(\theta)|\psi_i\rangle\right|^2$$
$$\approx \frac{1}{4}\left[r_{ii}^2 + r_{jj}^2 + 2r_{ii}r_{jj}\cos(\phi_{jj}-\phi_{ii}+\theta)\right] \qquad (B14)$$

so that we can measure it for different values of θ and directly obtain the phase difference between ϕ_{ii} and ϕ_{jj}. The definition of $\tilde{r}_{ij}$ will be modified accordingly.
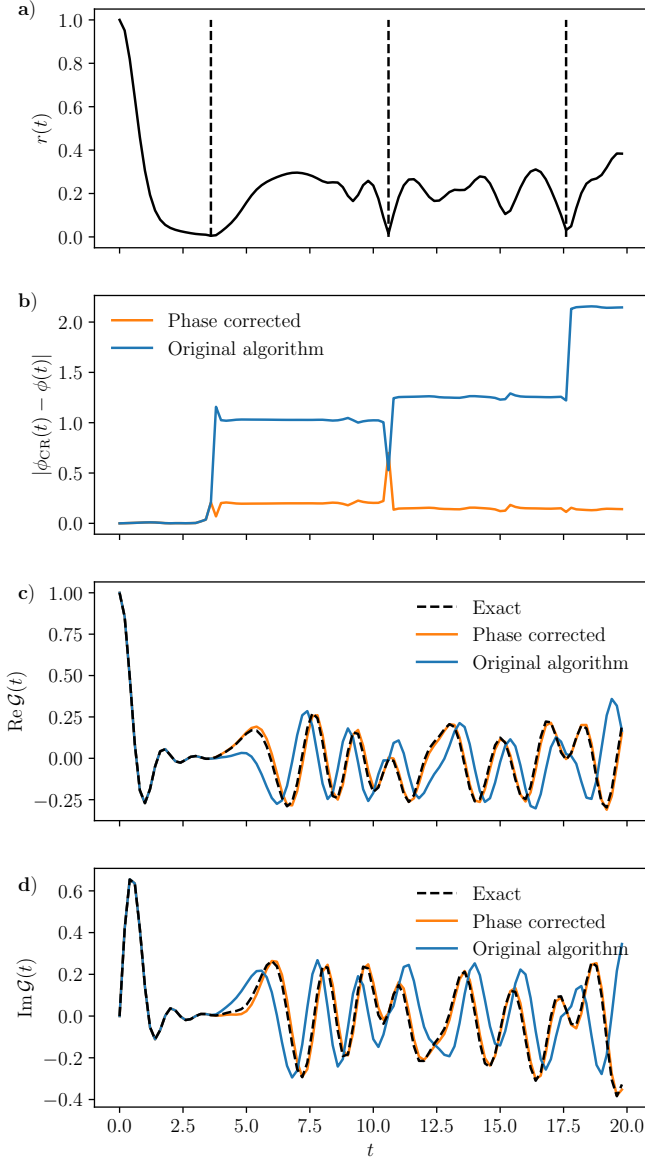
FIG. 5. An example of phase correction when $\mathcal{G}(t)$ is close to 0. Here the Hamiltonian coefficients are $(J, g) = (1, 1)$ and the initial state is still $|\psi\rangle = |\psi'\rangle = |\uparrow\uparrow \cdots\rangle$. The system size $N = 10$. The Trotter steps are $\tau = 0.2$ and $h = 0.01$. **(a)** The magnitude $r(t)$. The dashed lines indicate times at which $r(t)$ almost vanishes. **(b)** The phase difference between the estimated and the exact value. **(c-d)** The real and imaginary parts of $\mathcal{G}(t)$. Original algorithm corresponds to our algorithm described in main text. In the "phase corrected" results, we added a discrete phase jumpy π as well as a phase shift δ, which ensures continuity of the first derivative of $\mathcal{G}(t)$.

C. Zeros in Loschmidt amplitude

The Cauchy-Riemann equation for $\ln \mathcal{G}(z)$ holds only when $\mathcal{G}(z) \neq 0$. When $\mathcal{G}(z)$ crosses a zero at some time t_0, it is subject to a phase jump. In the case when we have access to arbitrary resolution and precision, the phase factor is $(-1)^{n_0}$, where n_0 is the smallest integer such that the n_0-th order derivative of $\mathcal{G}(z)$ is nonzero at t_0. This can be seen from the Taylor series expansion of $\mathcal{G}(z)$ at t_0:

$$\mathcal{G}(z) = \frac{1}{n_0!}\mathcal{G}^{(n_0)}(t_0)(z - t_0)^n + \mathcal{O}\left((z - t_0)^{n_0+1}\right). \text{ (C1)}$$

For a small $\epsilon > 0$., approximately

$$\mathcal{G}(t_0 - \epsilon) \approx (-1)^{n_0}\mathcal{G}(t_0 + \epsilon) \tag{C2}$$

and thus

$$\lim_{t \to t_0^+} \phi(t) \equiv \lim_{t \to t_0^-} \phi(t) + n_0\pi \pmod{2\pi}. \tag{C3}$$

In practice, with finite time resolution (e.g., the Trotter time), the gradient of the phase becomes singular near t_0 (or even some point where $\mathcal{G}(t)$ is almost zero). Even if we have included the $(-1)^{n_0}$ phase jump, this singularity can cause an additional phase factor $e^{i\delta}$ when going across t_0. Thus our algorithm will give a numerical result $\tilde{\mathcal{G}}(z)$, where

$$\tilde{\mathcal{G}}(t) = \begin{cases} \mathcal{G}(t), & t < t_0; \\ \mathcal{G}(t)e^{i\delta}, & t > t_0. \end{cases} \tag{C4}$$

It is possible to correct the phase error δ by requiring that the n_0-th derivative of $\mathcal{G}$ be continuous. In particular, we can directly estimate δ from the expression

$$e^{i\delta} = \lim_{t \to t_0^+} \tilde{\mathcal{G}}^{(n_0)}(t) / \lim_{t \to t_0^-} \tilde{\mathcal{G}}^{(n_0)}(t). \tag{C5}$$

In the discrete time setting, we evaluate the limits at the closest points on either side of the zero.

An example of the algorithm in the presence of small values of $r(t)$ is shown in Fig. 5. While there are no exact zeros in the Trotterized simulation, $r(t)$ becomes very small at the dashed lines in panel (a). In the original algorithm, this leads to large phase jumps because the discretization is too coarse. As shown in panels (b)–(c), it is possible to partially correct these jumps using the method described above, where we impose continuity of the first derivative close at the small values of $r(t)$.

D. Extension to multiple time evolution operators

It is possible to extend our algorithms to multiple time evolution operators:

$$\mathcal{G}(t_1, \cdots, t_n) = \langle\psi'|U_1O_1U_2O_2\cdots O_{n-1}U_n|\psi\rangle, \quad \text{(D1)}$$

where $U_j = e^{-iH_jt_j}$ and O_j are local unitaries.

- One can first switch on only U_1, i.e., set $t_2 = \cdots = t_n = 0$. Our algorithm works since the new intial state $O_1\cdots O_{n-1}|\psi\rangle$ still has finite correlation length.

- Then switch on U_2 as well. For each fixed t_1, perform our algorithm with initial state $O_2 \cdots O_{n-1} |\psi\rangle$, evolution operator $e^{-iH_2t_2}$ and final state $e^{iH_1t_1} |\psi'\rangle$. The phase at $t_2 = 0$ has already been determined in the previous step.

- Switch on the rest of the evolution unitaries one by one.

E. Numerical details

1. Quantum imaginary-time evolution of transverse field Ising chain

The Hamiltonian of the transverse field Ising model is given by

$$H = -J \sum_{i=1}^{N-1} S_i^z S_{i+1}^z + g \sum_{i=1}^{N} S_i^x. \tag{E1}$$

When applying $e^{\pm hH}$ on a product state $|\psi\rangle$ in the computational basis $\{ |\uparrow\rangle, |\downarrow\rangle \}^{\otimes N}$, it can be Trotterized as

$$|\psi_\pm\rangle \approx e^{\pm hH_2} e^{\pm hH_1} |\psi\rangle / c_\pm, \tag{E2}$$

where

$$H_1 = -J \sum_{i=1}^{N-1} S_i^z S_{i+1}^z, \quad H_2 = g \sum_{i=1}^{N} S_i^x. \tag{E3}$$

H_1 only leads to a rescaling factor $\exp(\pm h \langle\psi|H_1|\psi\rangle)$ but will not change the normalized state. For H_2, since

$$e^{aS^x} = \cosh\frac{a}{2}\mathbb{1} + \sinh\frac{a}{2}\sigma^x, \tag{E4}$$

it follows that

$$e^{\pm hgS_x} |\uparrow\rangle = \cosh\frac{hg}{2} |\uparrow\rangle \pm \sinh\frac{hg}{2} |\downarrow\rangle,$$
$$e^{\pm hgS_x} |\downarrow\rangle = \cosh\frac{hg}{2} |\downarrow\rangle \pm \sinh\frac{hg}{2} |\uparrow\rangle. \tag{E5}$$

Thus for each spin, there is an additional rescaling factor

$$\sqrt{\cosh^2\frac{hg}{2} + \sinh^2\frac{hg}{2}} = \sqrt{\cosh(hg)} \tag{E6}$$

and the spin is rotated by an angle

$$\theta = \arctan\tanh\frac{hg}{2}. \tag{E7}$$

The total rescaling factor is

$$c_\pm = e^{\pm h\langle\psi|H_1|\psi\rangle} \cdot \cosh(hg)^{\frac{N}{2}}. \tag{E8}$$

For the $|Z+\rangle = |\uparrow\uparrow\uparrow \cdots\rangle$ state,

$$c_\pm^{Z+} = \left[\exp\left(\mp\frac{hJ}{4} \cdot \frac{N-1}{N}\right)\sqrt{\cosh(hg)}\right]^N. \tag{E9}$$

2. Matrix product state simulations

In Fig. 2 of the main text, the imaginary-time evolution is described in section E 1. Given the normalized product states $|\psi_\pm\rangle$ from Eq. (E2), the real-time evolution is simulated with matrix product states (MPS) using the time-evolving block decimation (TEBD) algorithm of second order Trotterization. The bond dimension is chosen to be 200, which is sufficient for convergence in Fig. 2.

3. Discrete Fourier transform

As we only have access to the Loschmidt amplitude up to finite maximal time $t_{\max}$ and with finite resolution τ, we can only perform discrete (inverse) Fourier transform instead of the continuous one. Let $g_k = \mathcal{G}(k\tau)$ with $t_{\max} = K\tau$, where τ is the Trotter step. The discrete inverse Fourier transform of g_k has the form

$$d_l = \frac{\tau}{2\pi} \sum_{k=0}^{K-1} g_k e^{i2\pi kl/K}, \tag{E10}$$

for $0 \leq l \leq K-1$. For d_l to approximate the LDOS $d(l\eta)$ at energy $l\eta$, where η is the energy resolution, it should hold that

$$2\pi/K = \eta\tau, \tag{E11}$$

which gives

$$\eta = 2\pi/t_{\max}. \tag{E12}$$

In the case when $|\psi\rangle = |\psi'\rangle$, we additionally know that $\mathcal{G}(-t) = \mathcal{G}(t)^*$. Therefore the effective maximal evolution time is doubled and $\eta = \pi/t_{\max}$.

The range of energy is given by $K\eta = 2\pi/\tau$. The obtained discrete LDOS is periodic. We shift the range to include the mean energy of the initial product state.